
Task Aware Dreamer for Task Generalization in Reinforcement Learning

Chengyang Ying, Zhongkai Hao, Xinning Zhou, Hang Su, Songming Liu, Dong Yan, Jun Zhu

¹Department of Computer Science & Technology, Institute for AI, BNRist Center, Tsinghua-Bosch Joint ML Center, THBI Lab, Tsinghua University;

²Peng Cheng Laboratory

³ Tsinghua University-China Mobile Communications Group Co., Ltd. Joint Institute

Abstract

A long-standing goal of reinforcement learning is to acquire agents that can learn on training tasks and generalize well on unseen tasks that may share a similar dynamic but with different reward functions. A general challenge is to quantitatively measure the similarities between these different tasks, which is vital for analyzing the task distribution and further designing algorithms with stronger generalization. To address this, we present a novel metric named Task Distribution Relevance (TDR) via optimal Q functions of different tasks to capture the relevance of the task distribution quantitatively. In the case of tasks with a high TDR, i.e., the tasks differ significantly, we show that the Markovian policies cannot differentiate them, leading to poor performance. Based on this insight, we encode all historical information into policies for distinguishing different tasks and propose Task Aware Dreamer (TAD), which extends world models into our reward-informed world models to capture invariant latent features over different tasks. In TAD, we calculate the corresponding variational lower bound of the data log-likelihood, including a novel term to distinguish different tasks via states, to optimize reward-informed world models. Extensive experiments in both image-based control tasks and state-based control tasks demonstrate that TAD can significantly improve the performance of handling different tasks simultaneously, especially for those with high TDR, and demonstrate a strong generalization ability to unseen tasks.

1 Introduction

Deep Reinforcement Learning (DRL) has showcased impressive achievements across a multitude of challenges [26, 38, 18]. However, acquiring agents that excel in a variety of tasks, rather than mastering a specific task, remains challenging [54, 55, 19]. For example, an agent proficient in running might have difficulty walking, even though it appears to be an easier task. This tendency towards specialization harms the wider applicability of DRL in real-world scenarios. To address this issue, an increasing amount of research focuses on an extended setting where the agent is evaluated across a task distribution [46], which aims to train a generalizable agent capable of handling diverse and even unseen tasks. Numerous methodologies have been proposed with the aim of enhancing the agent’s generalization ability [16, 22, 32, 15]. However, the theoretical analysis of policy generalization ability remains largely unexplored, calling for further exploration and understanding.

In this study, our primary focus is on examining the connection between a policy’s generalization capacity, task distribution, and the expressiveness of the selected policy hypothesis set. Previous work [9] has shown that generalizing to unseen environments introduces partial observability, thus making all Markovian policies sub-optimal. However, these studies pay little attention to the

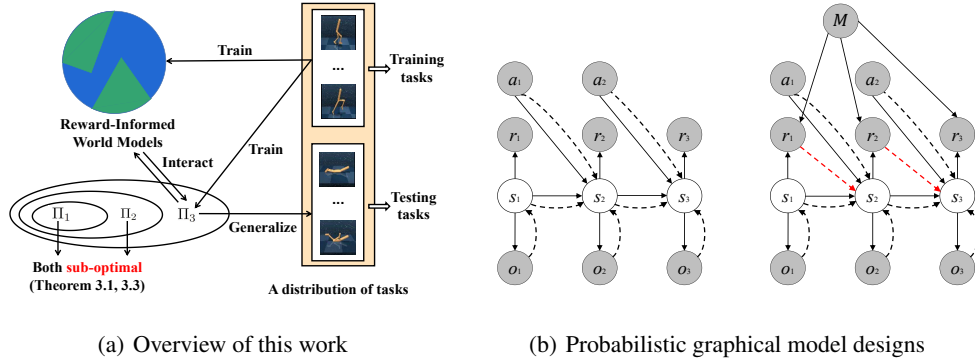


Figure 1: (a) **An overview.** Given a task distribution, we train the agent in training tasks and hope it to generalize to testing tasks. For improving the generalization, we propose TAD, which utilizes Π_3 to encode all historical information for inferring the current task and novel reward-informed world models for capturing invariant latent features. (b) Probabilistic graphical model designs for the single-task setting (**left**) and the task-distribution setting (**right**). The latter inspires the design of reward-informed world models. Solid and dashed lines represent the *generative process* and the *inference model*, respectively. We choose $q(s_t|s_{t-1}, a_{t-1}, o_t)$ [12] and $q(s_t|s_{t-1}, a_{t-1}, r_{t-1}, o_t)$ as inference models for the single-task setting and the task-distribution setting, respectively.

characteristics of task distribution and their impact on policy, which might be crucial for the design of generalizable agents.

To address this gap, we first propose a novel metric of Task Distribution Relevance (TDR), which encapsulates the relevance of different tasks within the distribution through their optimal Q functions. Furthermore, we prove that both the commonly adopted hypothesis set of Markovian policies Π_1 , and the set Π_2 of policies that encode historical states and actions, are *sub-optimal* under the task-distribution setting and struggle to generalize. This sub-optimality results from their inability to distinguish between different tasks, as well as the gap between their optimal performance and the optimal return tied to TDR. For task distributions with high TDR, the performance of traditional methods might degenerate significantly as they fail to identify the current task based on historical trajectories, a phenomenon we also empirically demonstrate in Sec. 5.

Therefore, we propose a novel method named Task Aware Dreamer (TAD) for handling different tasks simultaneously and generalizing to new tasks. Due to the sub-optimality of Π_1, Π_2 , TAD employs more expressive policies from Π_3 that encode all historical information including reward signals, for distinguishing different tasks. Furthermore, as current world models mainly focus on the single-task setting (left part of Fig. 1(b)), TAD extends world models [10, 12, 11], which can effectively learn the similar environment dynamics and capture invariant latent features across tasks [36, 50], into reward-informed world models. In particular, reward-informed world models are established with the probabilistic graphical model of the task-distribution setting (right part of Fig. 1(b)) and reward-informed inference policy. To train reward-informed world models, we calculate the variational lower bound of the log-likelihood on the sampled data, which includes a novel term for differentiating different tasks via states, as the training objective of TAD.

Extensive experiments are performed on image-based control task distributions based on DeepMind control suite [42] and state-based control task distributions simulated via MuJoCo simulator [43]. Agents are trained on fixed tasks and evaluated generalization ability on testing tasks that are unseen during training. Our results show that TAD can effectively distinguish different tasks to handle them simultaneously and significantly outperforms baselines, especially in tasks with high TDR. Furthermore, TAD shows strong sample efficiency and generalization ability in both image-based and state-based task distributions. In summary, our contributions are:

- To theoretically analyze the policy generalization ability under a distribution of tasks, we propose a novel metric TDR to measure the relevance of the task distribution. We further show that the Markovian policies are sub-optimal when handling the task distribution, and derive that the gap is related to the corresponding TDR.

- Since Markovian policies show poor performance and generalization in task distribution with high TDR, we propose novel reward-informed world models, which utilize historical information into policies and can capture invariant latent features between different tasks.
- By calculating the corresponding variational lower bound, we propose a novel algorithm named TAD to help the agent better generalize to unseen tasks, which demonstrates a strong generalization ability to unseen tasks compared with the alternative baselines.

2 Related Work

Generalization in Reinforcement Learning. Contemporary reinforcement learning methodologies consistently struggle when tasked with generalizing to new environments [54, 55, 40], a topic that has recently garnered substantial interest within the field. This is distinct from multi-task RL [51, 39, 24], which primarily aims for the trained agent to excel across all training tasks, or meta RL [6, 7, 33], which seeks to enable the trained agent to adapt rapidly to novel tasks. In contrast, generalization in RL aspires for the trained agent to perform proficiently across all training tasks while also extending its capabilities to unencountered tasks. To enhance agents’ generalization, various studies have empirically crafted an array of training methodologies, such as loss regularization [4, 16, 48], network architecture design [22, 31], and data augmentation [4, 32]. Despite this, there are few investigations into the mechanism behind policy generalization in unseen environments and its relationship with the distribution of those environments. Ghosh et al.[9] took the initial step in demonstrating that generalizing to unseen environments introduces partial observability, thereby rendering deterministic Markovian policies sub-optimal. In addition, some studies have experimentally indicated that stochastic or non-Markovian policies can yield superior generalization compared to deterministic and Markovian policies[23, 9]. Nevertheless, the expressive capabilities of differing hypothesis sets and their connection to the environment distribution remain understudied areas. This knowledge gap is significant for understanding current algorithms and for the design of more robust algorithms with enhanced generalization capacities.

World Models. The concept of world models, introduced by Ha et al. [10], aims to improve environmental learning for planning [12] and policy learning [11, 13]. Models like PlaNet [12] and Dreamer [11, 13, 14] utilize the Recurrent State Space Model (RSSM) to enhance the sample efficiency of visual control tasks. Subsequent research explored reconstruction-free [29, 5] world models, preserving representational capacity by avoiding the reconstruction of task-irrelevant elements. Also, techniques such as temporal predictive coding [28], cooperative reconstruction [8, 30], and Denoised MDP [49] have been proposed for more effective task-relevant information encoding. Recent works [1, 25, 34] integrate Transformer [45] into world models, improving performance by capturing long-term dependencies. Other studies propose using world models to extract environmental invariant features by learning from videos [37] or direct exploration [36, 50], and then fine-tuning to new tasks. However, most world models are designed for the single-task setting and struggle to manage multiple tasks at the same time without fine-tuning, limiting their effectiveness for zero-shot generalization to unseen tasks.

3 Task Distribution Relevance

In this part, we first formulate task generalization in RL and then analyze the performance of Markovian policies for handling a distribution of tasks via a novel metric Task Distribution Relevance.

3.1 Preliminary

We consider the setting with a task distribution \mathcal{T} of MDPs, where the agents need to solve tasks with the same dynamic and different reward functions. We might use environments or tasks interchangeably to refer to those MDPs in the rest of the paper. Formally, each MDP $\mathcal{M} \sim \mathcal{T}$ is represented as $\mathcal{M} = (\mathcal{S}, \mathcal{A}, \mathcal{P}, \mathcal{R}_{\mathcal{M}}, \gamma)$. Here \mathcal{S} and \mathcal{A} denote the state and action spaces, respectively. For $\forall (s, a) \in \mathcal{S} \times \mathcal{A}$, $\mathcal{P}(\cdot|s, a)$ is a distribution over \mathcal{S} , representing the dynamic of \mathcal{M} , and $\mathcal{R}_{\mathcal{M}}(s, a)$ is the reward function of \mathcal{M} . Furthermore, $\gamma \in (0, 1)$ is a discount factor.

Now we introduce 3 different types of policy hypothesis sets. As we will show in Sec. 3.2, even though the Markovian policy set is enough for the traditional single-task setting, we need to consider the other two policy hypothesis sets to deal with the more challenging setting of task distribution.

1. Markovian policy set Π_1 [41, 21, 52], i.e., $\Pi_1 = \{\pi | \pi : \mathcal{S} \rightarrow \mathcal{D}(\mathcal{A})\}$, here $\mathcal{D}(\mathcal{A})$ represents a distribution over \mathcal{A} , which is widely used and optimal for handling single environment;
2. \mathcal{S} - \mathcal{A} memorized policy set Π_2 [11, 13, 23], i.e., $\Pi_2 = \{\pi | \pi : \mathcal{H} \rightarrow \mathcal{D}(\mathcal{A})\}$, here $\mathcal{H} = \bigcup_{t=1}^{\infty} \mathcal{H}_t$, $\mathcal{H}_t = (\mathcal{S} \times \mathcal{A})^{t-1} \times \mathcal{S}$;
3. \mathcal{S} - \mathcal{A} - \mathcal{R} memorized policy set Π_3 [47, 20, 33], i.e., $\Pi_3 = \{\pi | \pi : \mathcal{I} \rightarrow \mathcal{D}(\mathcal{A})\}$, here $\mathcal{I} = \bigcup_{t=1}^{\infty} \mathcal{I}_t$, $\mathcal{I}_t = (\mathcal{S} \times \mathcal{A} \times \mathbb{R})^{t-1} \times \mathcal{S}$.

Naturally we have $\Pi_1 \subseteq \Pi_2 \subseteq \Pi_3$, as illustrated in Fig. 1(a). Given the policy $\pi \in \Pi_3$, at each timestep t , the agent will use the history information $(s_0, a_0, r_0, s_1, a_1, r_1, \dots, s_t)$ to sample action a_t , arrive at the next state $s_{t+1} \sim \mathcal{P}(\cdot | s_t, a_t)$, and get the current return $r_t = \mathcal{R}_{\mathcal{M}}(s_t, a_t)$. The performance of policy π in \mathcal{M} is defined as the expectation of the discounted return of the trajectory τ : $J_{\mathcal{M}}(\pi) = \mathbb{E}_{\tau \sim \pi} [R(\tau) \triangleq \sum_{t=0}^{\infty} \gamma^t r_t]$, where $R(\tau)$ represents the discounted return of τ . Given \mathcal{T} , we hope to find the optimal policy over all tasks sampled from \mathcal{T} , i.e., $\max_{\pi} \mathbb{E}_{\mathcal{M} \sim \mathcal{T}} J_{\mathcal{M}}(\pi)$. We denote $J_{\mathcal{T}}^* \triangleq \mathbb{E}_{\mathcal{M} \sim \mathcal{T}} [\max_{\pi} J_{\mathcal{M}}(\pi)]$ as the optimal return under \mathcal{T} , and $J_{\mathcal{T}}^i \triangleq \max_{\pi \in \Pi_i} [\mathbb{E}_{\mathcal{M} \sim \mathcal{T}} J_{\mathcal{M}}(\pi)]$ as the optimal return for Π_i ($i = 1, 2, 3$) under \mathcal{T} .

It is well known that the optimal policy for any fully-observed single task belongs to the minimal set Π_1 . Nevertheless, when considering the generalization of agents in the more challenging setting, previous work [9] has shown that the fully-observed environment will be partially observable and Π_1 is no longer optimal, i.e., in some cases $J_{\mathcal{T}}^1 < J_{\mathcal{T}}^*$. Also, [23] empirically finds that encoding historical states and actions into the policy, i.e., using the hypothesis set Π_2 , can gain better generalization than Markovian policies since Π_2 can handle partial observability to some extent. However, the gap between $J_{\mathcal{T}}^1$ and $J_{\mathcal{T}}^*$ as well as its connection with the task distribution \mathcal{T} are still unclear. We aim to address this issue by first proposing an effective metric of \mathcal{T} for evaluating this gap and further analyzing these policy hypothesis sets.

3.2 Theoretical Analyses

Our first main result shows that, although $\Pi_1 \subseteq \Pi_2$, they own the same expressive ability, i.e., $J_{\mathcal{T}}^1 = J_{\mathcal{T}}^2$, and are both *sub-optimal*, as summarized below.

Theorem 1 (Sub-Optimality of Π_1, Π_2 , Proof in Appendix B.1). *We set $\bar{\mathcal{M}} = (\mathcal{S}, \mathcal{A}, \mathcal{P}, \bar{\mathcal{R}}, \gamma)$, here $\bar{\mathcal{R}} = \mathbb{E}_{\mathcal{M} \sim \mathcal{T}} [\mathcal{R}_{\mathcal{M}}]$. For $\forall \pi \in \Pi_2$, we have $\mathbb{E}_{\mathcal{M} \sim \mathcal{T}} [J_{\mathcal{M}}(\pi)] = J_{\bar{\mathcal{M}}}(\pi)$ and further $J_{\mathcal{T}}^1 = J_{\mathcal{T}}^2 \leq J_{\mathcal{T}}^*$.*

Theorem 1 reveals that the cumulative returns of policies in Π_1 and Π_2 are the same as their returns in the ‘‘average’’ MDP $\bar{\mathcal{M}}$, where the reward function is the average of reward functions in different tasks. Also, Π_1 and Π_2 cannot distinguish different tasks and are both *sub-optimal*, as the policies in them choose actions via current state or historical state-action pairs, which are the same in all tasks.

To further quantitatively investigate the gap between $J_{\mathcal{T}}^1, J_{\mathcal{T}}^2$ and $J_{\mathcal{T}}^*$, we propose a novel metric named Task Distribution Relevance (TDR) of the distribution \mathcal{T} as

Definition 1 (Task Distribution Relevance). *For any task distribution \mathcal{T} and state s , the Task Distribution Relevance of \mathcal{T} and s is defined as*

$$D_{TDR}(\mathcal{T}, s) = \mathbb{E}_{\mathcal{M} \sim \mathcal{T}} [\max_a Q_{\mathcal{M}}^*(s, a)] - \max_a \mathbb{E}_{\mathcal{M} \sim \mathcal{T}} [Q_{\mathcal{M}}^*(s, a)]. \quad (1)$$

Intuitively, TDR describes the relevance of \mathcal{T} by using optimal Q functions, which determine the distribution of optimal actions in corresponding tasks. Based on TDR, we are able to bound the gap:

Theorem 2 (Proof in Appendix B.2). *Assume $\pi_{\mathcal{M}}^* = \arg \max_{\pi} J_{\mathcal{M}}(\pi)$, for $\forall \pi \in \Pi_1$, we have*

$$J_{\mathcal{T}}^* - \mathbb{E}_{\mathcal{M} \sim \mathcal{T}} [J_{\mathcal{M}}(\pi)] = \mathbb{E}_{\mathcal{M} \sim \mathcal{T}} [J_{\mathcal{M}}(\pi_{\mathcal{M}}^*) - J_{\mathcal{M}}(\pi)] \geq \frac{1}{1-\gamma} \mathbb{E}_{s \sim d_{\mathcal{M}, \pi}} [D_{TDR}(\mathcal{T}, s)]. \quad (2)$$

Thus we have $J_{\mathcal{T}}^* - J_{\mathcal{T}}^2 = J_{\mathcal{T}}^* - J_{\mathcal{T}}^1 \geq \frac{1}{1-\gamma} \mathbb{E}_{s \sim d_{\mathcal{M}, \pi^*}} [D_{TDR}(\mathcal{T}, s)]$, here $\pi^* = \arg \max_{\pi \in \Pi_1} J_{\mathcal{M}}(\pi)$.

Theorem 2 demonstrates that the gap between $J_{\mathcal{T}}^1$, $J_{\mathcal{T}}^2$ and $J_{\mathcal{T}}^*$ is related to the TDR of \mathcal{T} . When considering \mathcal{T} with high TDR, i.e., the optimal Q values in different tasks differ greatly, the performance of Π_1 and Π_2 will be extremely poor since they cannot differentiate different tasks and their expressive abilities are significantly limited. This conclusion is further verified empirically in Sec. 5. Moreover, we can show that $J_{\mathcal{T}}^1$, $J_{\mathcal{T}}^2$ might be arbitrarily small when $J_{\mathcal{T}}^3$ might be arbitrarily close to $J_{\mathcal{T}}^*$ (More details are in Appendix B.4), which demonstrates that Π_3 owns stronger expressive ability. Consequently, it is necessary to utilize reward information, i.e., choosing policies from Π_3 , to distinguish different tasks for enhancing expression ability and generalization over the task distribution.

4 Task Aware Dreamer

To address the sub-optimality of policy sets Π_1 , Π_2 and enhance the generalization ability to unseen tasks, we introduce Task Aware Dreamer (TAD) to utilize Π_3 to differentiate different tasks by encoding all historical information, including reward signals, into policies. Moreover, TAD incorporates ideas of Dreamer-oriented world models [10, 11] to extract invariant latent features [36, 50] for improving the sample efficiency and generalization capacity. We provide the brief pseudo code of TAD in Algorithm 1 (the detailed version is in Appendix A).

Formally, given the task distribution \mathcal{T} , we sample M training tasks $\{\mathcal{M}_m\}_{m=1}^M$ for optimizing the agent and hope it can generalize to N unseen testing tasks $\{\mathcal{M}_{M+n}\}_{n=1}^N$ sampled from \mathcal{T} . Since the distribution is unknown and hard to calculate, TAD trains the agent in training tasks, i.e., maximizing $\frac{1}{M} \sum_{m=1}^M J_{\mathcal{M}_m}(\pi)$ and evaluate it in testing tasks, i.e., evaluating $\frac{1}{N} \sum_{n=1}^N J_{\mathcal{M}_{M+n}}(\pi)$. As the dynamics of training tasks and testing tasks are the same, TAD employs Dreamer-oriented world models [10, 11], i.e., Recurrent State Space Model (RSSM) [12], to model the environment dynamic and capture invariant latent features.

As existing world models mainly focus on the single-task setting, in Sec. 4.1, we expand them into our reward-informed world models, which are based on the task-distribution setting and incorporate reward-informed hypothesis set Π_3 as the inference model. Then we delve into the training of TAD in detail, including the optimization of reward-informed world models and the actor-critic, in Sec. 4.2.

4.1 Reward-Informed World Models

To build reward-informed world models, we first analyze the probabilistic graphical model of the task-distribution setting in Fig. 1(b), where the reward does not only rely on the previous states and actions but also on the current task. In this setting, the joint distribution can be calculated as follows

$$p(s_{1:T}, o_{1:T}, r_{1:T}, a_{1:T-1}, \mathcal{M}) = p(\mathcal{M}) \prod_{t=1}^T p(s_{t+1}|s_t, a_t) p(o_t|s_t) p(r_t|s_t, \mathcal{M}), \quad (3)$$

and we choose the reward-informed inference model by Π_3 to approximate state posteriors as

$$q(s_{1:T}|o_{1:T}, a_{1:T}, r_{1:T}) = \prod_{t=1}^T q(s_t|s_{t-1}, a_{t-1}, r_{t-1}, o_t). \quad (4)$$

Inspired by previous work [12], we further construct the variational lower bound of the log-likelihood on the data as

$$\begin{aligned} & \ln p(o_{1:T}, r_{1:T}, \mathcal{M}|a_{1:T}) \\ & \geq \sum_{t=1}^T \mathbb{E}_{q(s_t|o_{\leq t}, a_{< t}, r_{< t})} [\ln p(o_t, r_t|\mathcal{M}, s_t) - \text{KL}(q(s_t|o_{\leq t}, r_{< t}, a_{< t})||p(s_t|s_{t-1}, a_{t-1}))] \\ & \quad + \mathbb{E}_{q(s_{1:T}|o_{1:T}, a_{1:T}, r_{1:T})} [\ln p(\mathcal{M}|s_{1:T})]. \end{aligned} \quad (5)$$

The detailed derivation is provided in Appendix B.4. Here the first two terms in the lower bound are for reconstructing observations, predicting rewards, and inferring states, which are similar to the results in the single-task setting [12]. And the last term is dedicated to predicting the current task from historical information, which is beneficial for improving the generalization since they encourage

Algorithm 1 Task Aware Dreamer (TAD)

Require: M training tasks $\{\mathcal{M}_m\}_{m=1}^M$, M replay buffers $\{\mathcal{D}_m\}_{m=1}^M$, N testing tasks $\{\mathcal{M}_{M+n}\}_{n=1}^N$, initialize parameters of world models, the policy, and the critic.

- 1: **while** not converge **do**
 - 2: **for** update step = 1, 2, ..., U **do**
 - 3: Sample o - a - r pairs $\{(o_t^i, a_t^i, r_t^i)_{t=1}^T\}$ from each replay buffer $\mathcal{D}_i, i = 1, 2, \dots, M$
 - 4: Calculate the deterministic state h and further calculate model states s .
 - 5: Update the world models via optimizing Eq. (6).
 - 6: Collect imagined trajectories from each s via the policy and the world models and use these imagined trajectories to update the policy and the critic.
 - 7: **end for**
 - 8: Collect trajectories from $\mathcal{M}_m (m = 1, 2, \dots, M)$ and store them into the replay buffer \mathcal{D}_m .
 - 9: **end while**
 - 10: Evaluate the agent in testing environments $\mathcal{M}_{M+n} (n = 1, 2, \dots, N)$.
-

inferring the current task context. Following RSSM and Eq.(5), our reward-informed world models consist of the following components:

$$\begin{aligned} \text{Deterministic state model: } & h_t = f(h_{t-1}, s_{t-1}, a_{t-1}, r_{t-1}), & \text{Transition model: } & p_\theta(s_t|h_t), \\ \text{Observation model: } & p_\theta(o_t|h_t, s_t), & \text{Reward model: } & p_\theta(r_t|h_t, s_t), \\ \text{Task model: } & p_\theta(\mathcal{M}|h_t, s_t). \end{aligned}$$

Specifically, the deterministic state model encodes historical states, actions, and rewards into current hidden features, by using gated recurrent unit (GRU) [2, 3] as $f(\cdot) = \text{GRU}(\cdot)$. It is worth noting that $f(\cdot)$ also can be easily extended to other architectures like Transformer [45]. Then the transition model, observation model, and reward model, which are the same as RSSM, further predict state, observation, and reward respectively. Finally, the task model infers the current task in order to distinguish trajectories from different tasks.

4.2 Optimization

Based on the above analyses, we now introduce the training of TAD in detail. Following previous work [11], we adopt an alternating training approach between the reward-informed world models and the policy, which is a parameterized neural network $\pi_\phi(\cdot|h_t, s_t)$.

In the stage of collecting data, TAD utilizes different replay buffers $\mathcal{D}_1, \mathcal{D}_2, \dots, \mathcal{D}_M$ to store sampled trajectories from given training tasks $\mathcal{M}_1, \mathcal{M}_2, \dots, \mathcal{M}_M$, respectively. Then in the training stage, TAD will sample data from each replay buffer and the training objective of the reward-informed world models in TAD is followed Eq. (5) as

$$\begin{aligned} L_{\text{TAD}} = & \sum_{i=1}^M \mathbb{E}_q \left[\sum_{t=1}^T \ln p_\theta(o_t^i|h_t^i, s_t^i) + \sum_{t=1}^T \ln p_\theta(r_t^i|h_t^i, s_t^i) \right. \\ & \left. - \sum_{t=1}^T D_{\text{KL}}(q(s_t^i|h_t^i, o_t^i)||p_\theta(s_t^i|h_t^i)) + \sum_{t=1}^T \ln p_\theta(\mathcal{M}_i|h_t^i, s_t^i) \right]. \end{aligned} \quad (6)$$

Here the first three items in Eq. (6) are similar to Dreamer for reconstructing observations, predicting rewards, and inferring states. The novel last term in Eq. (6) is calculated in Eq. (5) for encouraging the agent to encode task information into hidden states and infer the current task based on these hidden states, which is beneficial for generalizing to unseen tasks.

In terms of training the actor-critic, both of which are parameterized neural networks, we follow the actor-critic learning approach in Dreamer [11] with a more powerful hypothesis set Π_3 , which encodes reward signals into policies and further uses states to predict the task for improving the generalization. When optimizing the policy, TAD samples a series of states from the replay buffer and starts from them to imagine trajectories via interacting with reward-informed world models, which is fixed at this time. Here the reward-informed world models can capture the invariant features, which are beneficial for the agent to train more effectively and gain better generalization. After obtaining imagined trajectories, the agent can be optimized via maximizing the λ -return [35] and the critic can be optimized via regressing the targets calculated by the temporal difference algorithm [41].

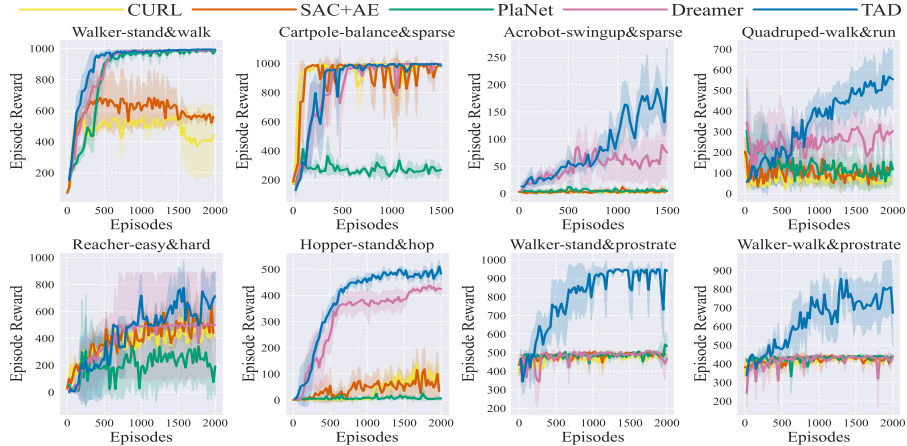


Figure 2: Average cumulative reward curves over different task combinations in DMC for CURL, SAC+AE, PlaNet, Dreamer, and TAD. The x-axes indicate the number of episodes interacting with the environment, and the y-axes indicate the performance, including average rewards with std.

5 Experiments

5.1 Experimental Setup

Image-based Control. To demonstrate the superiority of TAD and verify analyses about TDR in Sec. 3, we first consider lots of different task combinations [27] in DeepMind control suite (DMC) [42]. These task combinations include (1) four task combinations of **Walker-stand&walk** [27], **Cartpole-balance&sparse**, **Acrobot-swingup&sparse** and **Quadruped-walk&run**, all of which share the same optimal actions with TDR being 0; (2) two task combinations with low TDR of **Reacher-easy&hard** [27] and **Hopper-stand&hop**; and (3) another two task combinations with high TDR of **Walker-stand&prostrate** and **Walker-walk&prostrate**. For example, Walker-stand and Walker-prostrate hope a two-leg robot to maintain its height above a certain threshold and below another certain threshold respectively, yielding almost opposite optimal Q functions with huge TDR. More details about them are in Appendix C.

Additionally, we design three task distributions by extending tasks from DeepMind control suite to evaluate algorithms’ generalization: (1) **Cheetah_speed**(α, β), which is based on the task Cheetah-run and hopes the agent run within the target speed interval ($\alpha - \beta, \alpha + \beta$); (2) **Pendulum_angle**(α, β), which is based on the task Pendulum-swingup and hopes an inverted pendulum stay its pole within the target angle interval ($\arccos \alpha, \arccos \beta$); and (3) **Quadruped_speed**(α, β), which is based on the task Quadruped-run and requires the quadruped agent run within the target speed interval ($\alpha - \beta, \alpha + \beta$). For each task distribution, we sample 4 tasks as training tasks and 2 additional tasks as testing tasks. More detailed descriptions of these task distributions are also in Appendix C.

State-based Control. To demonstrate the scalability of TAD, we also consider some state-based continuous control task distributions about robotic locomotion, simulated via the MuJoCo simulator [43]. In accordance with [7, 33], our chosen tasks distributions include (1) **Half-Cheetah-Fwd-Back**, which includes two opposite tasks; and (2) **Half-Cheetah-Vel** and **Humanoid-Direc-2D**, which are task distributions and we sample 100 tasks for training as well as 30 tasks for testing. More details of these task distributions are in Appendix D.

Baselines. In image-based control, we compare TAD with two model-free methods: CURL [21] and SAC+AE [52]. These methods employ Markovian policies and belong to Π_1 . In addition, we compare TAD with two classic world models, PlaNet [12] and Dreamer [11], both of which utilize all historical state-actions for decision-making and belong to Π_2 . In state-based control, we employ PlaNet and Dreamer as baselines. Moreover, we take some meta RL methods like MAML [7], RL2 [6], and PEARL [33], which are few-shot adaptation, as reference.

Metrics. For the multi-task setting, we evaluate the average return of all tasks. For the task generalization setting, we train agents in training tasks and evaluate them in both training and testing

Tasks	Walker-stand&walk	Cartpole-balance&sparse	Acrobot-swingup&sparse	Quadruped-walk&run
CURL	563.4 ± 16.0	996.8 ± 0.8	6.9 ± 3.4	203.3 ± 69.9
SAC+AE	683.8 ± 164.3	993.4 ± 0.6	11.7 ± 5.4	203.2 ± 70.2
PlaNet	990.6 ± 3.8	412.8 ± 65.9	12.2 ± 9.8	305.3 ± 206.6
Dreamer	992.3 ± 1.7	997.1 ± 1.1	89.3 ± 58.0	345.4 ± 218.3
TAD	994.6 ± 0.1	997.3 ± 0.7	194.7 ± 72.5	571.2 ± 131.4

Tasks	Reacher-easy&hard	Hopper-stand&hop	Walker-stand&prostrate	Walker-walk&prostrate
CURL	552.5 ± 88.9	137.1 ± 9.2	496.3 ± 8.7	441.0 ± 7.7
SAC+AE	669.5 ± 99.4	118.2 ± 83.1	504.4 ± 6.7	445.8 ± 2.6
PlaNet	341.0 ± 228.3	25.9 ± 25.7	544.3 ± 68.6	445.4 ± 5.1
Dreamer	506.1 ± 382.9	436.9 ± 18.9	510.0 ± 6.7	449.7 ± 12.5
TAD	775.2 ± 203.1	510.7 ± 22.8	951.0 ± 2.8	855.3 ± 56.2

Table 1: Performance (mean ± std) over different task combinations in DMC of the best policy. Numbers greater than **95 %** of the best performance for each environment are **bold**.

Tasks	Cheetah_speed		Pendulum_angle		Quadruped_speed	
	Train	Test	Train	Test	Train	Test
CURL	211.7 ± 13.7	57.4 ± 26.6	137.1 ± 8.6	57.4 ± 21.8	7.6 ± 4.4	2.3 ± 1.0
SAC+AE	182.2 ± 7.6	115.2 ± 10.1	144.0 ± 4.5	68.6 ± 3.7	6.7 ± 6.4	1.5 ± 0.7
PlaNet	176.6 ± 25.9	83.0 ± 52.2	99.8 ± 28.3	80.5 ± 24.2	24.8 ± 17.5	7.9 ± 5.8
Dreamer	250.2 ± 9.6	3.0 ± 2.2	92.2 ± 19.9	79.6 ± 14.8	28.3 ± 1.1	20.1 ± 1.0
TAD	956.8 ± 6.0	787.4 ± 163.6	287.3 ± 22.8	126.6 ± 31.8	37.6 ± 3.1	39.6 ± 3.0

Table 2: Performance (mean ± std) over different task distributions in DMC of the best policy. For each task distribution, we train agents in the train tasks and evaluate them in both train and test tasks. Numbers greater than **95 %** of the best performance for each environment are **bold**.

tasks. For all experiments, we train 3 policies with different seeds and calculate the mean and standard deviations to mitigate the effects of randomness caused by stochastic environments and policies.

5.2 Experimental Results for TDR

Firstly, to validate our analyses of TDR and demonstrate the effectiveness of TAD, we present the results of the multi-task setting. We depict the mean and standard deviations of returns as functions of the episode number in the training stage in Fig. 2, where the solid line and the lighter part represent the mean and standard deviations respectively. Also, we report the optimal mean ± standard deviations of the average cumulative return of all environments in Table 1.

As shown in Table 1 and Fig. 2, TAD outperforms baselines in all environments, especially in those with high TDR. In tasks where TDR is 0, like Walker-stand&walk and Cartpole-balance&sparse, the optimal performance of TAD and baselines are similar since these tasks share the same optimal action and Π_1, Π_2 own the optimal policy, as derived in Theorem 2. In these cases, TAD still converges faster and shows more robust performance. In Acrobot-swingup&sparse and Quadruped-walk&run, although TDR of these tasks is 0, TAD can surpass baselines since it can better distinguish different tasks. Finally, in the last four environments with non-zero TDR, TAD achieves a notable improvement compared with baselines. Especially, in Walker-stand&prostrate and Walker-walk&prostrate, where TDR is significantly huge, baselines perform poorly as these policies belong to Π_1, Π_2 and can not differentiate different tasks, which also aligns with our Theorem 2. In contrast, TAD can distinguish between tasks by utilizing reward signals and improves performance conspicuously.

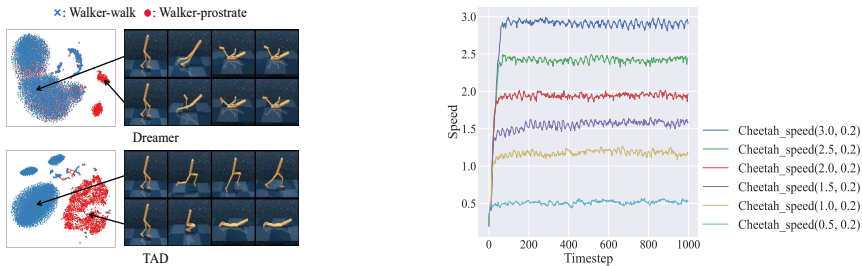
5.3 Experimental Results for Task Generalization

Furthermore, we report the results of the task generalization setting to demonstrate that our TAD can effectively generalize the agent to unseen tasks via encoding the reward information. In Table 2, we report the optimal result of training tasks as well as testing tasks in environments mentioned in Sec. 5.1. As shown in Table 2, TAD can significantly enhance the average cumulative return in both training tasks and testing tasks compared with baselines. This suggests that TAD can both handle multiple training tasks simultaneously and generalize to unseen testing tasks effectively.

Additionally, following the setting of [7, 33], we also evaluate TAD in state-based robotic locomotion tasks based on MuJoCo simulator [43]. For each environment, we set the length of episodes to 200 and report the optimal result of training tasks as well as testing tasks of PlaNet, Dreamer, and TAD in Table 3. We also compare them with classical meta RL methods like MAML [7], RL2 [6], and

Tasks	Half-Cheetah-Fwd-Back	Half-Cheetah-Vel		Humanoid-Direc-2D	
	Train&Test	Train	Test	Train	Test
PlaNet	30.5 ± 42.9	-198.1 ± 1.9	-202.1 ± 1.8	215.9 ± 72.3	220.6 ± 75.3
Dreamer	127.4 ± 181.8	-151.4 ± 0.4	-169.4 ± 1.2	260.5 ± 48.9	263.5 ± 52.3
TAD	1455.8 ± 78.3	-49.3 ± 1.9	-47.1 ± 0.3	298.9 ± 95.1	299.2 ± 91.9
MAML	429.3 ± 81.4	—	-121.0 ± 37.1	—	205.3 ± 34.7
RL2	1006.9 ± 26.4	—	-146.9 ± 0.4	—	268.8 ± 30.2
PEARL	1912.2 ± 41.5	-28.6 ± 1.2	-29.6 ± 1.1	964.6 ± 2.3	966.5 ± 3.3

Table 3: Performance (mean ± std) over different task distributions in MuJoCo of the best policy. For each task distribution, agents are trained in train tasks and evaluated in both train and test tasks. Numbers greater than **95%** of the best performance are **bold**. Results of three meta RL methods (MAML, RL2, and PEARL), which are **few-shot adaptation** in testing, are also provided as reference.



(a) T-SNE of all states via Dreamer and TAD

(b) Speeds of TAD agents in different tasks

Figure 3: (a) Visualization of Dreamer (upper subfigure) and TAD (below subfigure) for handling Walker-walk&Prostrate. For each algorithm in each task, we show 4 frame observations of a trajectory in the right part. In the left part, we draw t-SNE [44] results of all states in trajectories of Walker-walk (blue points) and Walker-prostrate (red points). (b) Visualization of the trained TAD agent in the task distribution of Cheetah_speed. We plot the speed of the agent as a function of timesteps in all tasks.

PEARL [33], which adapt to new tasks with few-shot learning during testing. As shown in Table 3, TAD can achieve a significant improvement in the average cumulative return for both training tasks and testing tasks, since TAD is aware of task information and can generalize to unseen tasks.

5.4 Visualization Results

In this part, we present some visualization to better understand how TAD works. First, we sample trajectories from the trained agent via Dreamer as well as TAD in Walker-walk&prostrate and visualize some observations (right part of Fig. 3(a)) as well as all states (left part of Fig. 3(a)), of which the dimensions are reduced for visualization by t-SNE [44]. As shown here, states in TAD of different tasks are clearly distinguished, while Dreamer can not differentiate them and perform the same in different tasks. Consequently, TAD can successfully distinguish different tasks and handle them at the same time effectively. Videos of these trajectories are provided in supplementary materials.

Moreover, for each task sampled from the task distribution Cheetah_speed (here parameters (3.0, 0.2), (2.0, 0.2), (1.5, 0.2), (0.5, 0.2) are for training tasks and parameters (2.5, 0.2), (0.5, 0.2) are for testing tasks), we plot the speed of the agent as a function of the timestep in Fig. 3(b). As depicted, for each task, the agent trained by TAD will quickly improve its speed until reaching the target speed and then keep its speed since the speed determines whether it has met the task requirements via utilizing historical information. Consequently, TAD is aware of different tasks and can successfully generalize to unseen test tasks. We also provide videos of these trajectories in supplementary materials.

5.5 Limitations and Discussion

In terms of limitations, TAD needs the assumption that the task context is continuously related to historical information for generalizing to unseen tasks. As a result, TAD might be difficult to generalize in sparse-reward settings. We further demonstrate that without extra knowledge or finetuning, zero-shot generalization to unseen tasks with extremely sparse rewards is impossible since there is no way to distinguish different tasks (more details are in Appendix B.5). Fortunately, in the setting with relatively sparse reward, we also conducted studies in Appendix E to show that TAD can better infer the current task via historical information and generalize to unseen tasks than baselines.

6 Conclusion

In this work, we propose a novel metric Task Distribution Relevance (TDR) to capture the relevance of the task distribution and show that Markovian policies perform poorly in tasks with high TDR. Moreover, for improving generalization over tasks, we propose a novel framework of Task Aware Dreamer (TAD) which distinguishes different tasks via all historical information and utilizes novel reward-informed world models to capture invariant latent features. In TAD, we calculate the corresponding variational lower bound of the log-likelihood on data, which includes a novel loss term to distinguish different tasks via states. Experimental results in image-based and state-based control task distributions demonstrate that TAD can remarkably improve the performance of handling different tasks simultaneously, especially for high TDR ones, and successfully generalize to unseen tasks.

References

- [1] Chang Chen, Jaesik Yoon, Yi-Fu Wu, and Sungjin Ahn. Transdreamer: Reinforcement learning with transformer world models. In *Deep RL Workshop NeurIPS 2021*, 2021.
- [2] Kyunghyun Cho, Bart van Merriënboer, Dzmitry Bahdanau, and Yoshua Bengio. On the properties of neural machine translation: Encoder–decoder approaches. In *8th Workshop on Syntax, Semantics and Structure in Statistical Translation, SSST 2014*, pages 103–111. Association for Computational Linguistics (ACL), 2014.
- [3] Junyoung Chung, Caglar Gulcehre, KyungHyun Cho, and Yoshua Bengio. Empirical evaluation of gated recurrent neural networks on sequence modeling. *arXiv preprint arXiv:1412.3555*, 2014.
- [4] Karl Cobbe, Oleg Klimov, Chris Hesse, Taehoon Kim, and John Schulman. Quantifying generalization in reinforcement learning. In *International Conference on Machine Learning*, pages 1282–1289. PMLR, 2019.
- [5] Fei Deng, Ingook Jang, and Sungjin Ahn. Dreamerpro: Reconstruction-free model-based reinforcement learning with prototypical representations. In *International Conference on Machine Learning*, pages 4956–4975. PMLR, 2022.
- [6] Yan Duan, John Schulman, Xi Chen, Peter L Bartlett, Ilya Sutskever, and Pieter Abbeel. RI^2 : Fast reinforcement learning via slow reinforcement learning. *arXiv preprint arXiv:1611.02779*, 2016.
- [7] Chelsea Finn, Pieter Abbeel, and Sergey Levine. Model-agnostic meta-learning for fast adaptation of deep networks. In *International conference on machine learning*, pages 1126–1135. PMLR, 2017.
- [8] Xiang Fu, Ge Yang, Pulkit Agrawal, and Tommi Jaakkola. Learning task informed abstractions. In *International Conference on Machine Learning*, pages 3480–3491. PMLR, 2021.
- [9] Dibya Ghosh, Jad Rahme, Aviral Kumar, Amy Zhang, Ryan P Adams, and Sergey Levine. Why generalization in rl is difficult: Epistemic pomdps and implicit partial observability. *Advances in Neural Information Processing Systems*, 34:25502–25515, 2021.
- [10] David Ha and Jürgen Schmidhuber. World models. *arXiv preprint arXiv:1803.10122*, 2018.
- [11] Danijar Hafner, Timothy Lillicrap, Jimmy Ba, and Mohammad Norouzi. Dream to control: Learning behaviors by latent imagination. In *International Conference on Learning Representations*, 2019.
- [12] Danijar Hafner, Timothy Lillicrap, Ian Fischer, Ruben Villegas, David Ha, Honglak Lee, and James Davidson. Learning latent dynamics for planning from pixels. In *International conference on machine learning*, pages 2555–2565. PMLR, 2019.
- [13] Danijar Hafner, Timothy P Lillicrap, Mohammad Norouzi, and Jimmy Ba. Mastering atari with discrete world models. In *International Conference on Learning Representations*, 2020.
- [14] Danijar Hafner, Jurgis Pasukonis, Jimmy Ba, and Timothy Lillicrap. Mastering diverse domains through world models. *arXiv preprint arXiv:2301.04104*, 2023.
- [15] Nicklas Hansen and Xiaolong Wang. Generalization in reinforcement learning by soft data augmentation. In *2021 IEEE International Conference on Robotics and Automation (ICRA)*, pages 13611–13617. IEEE, 2021.
- [16] Maximilian Igl, Kamil Ciosek, Yingzhen Li, Sebastian Tschiatschek, Cheng Zhang, Sam Devlin, and Katja Hofmann. Generalization in reinforcement learning with selective noise injection and information bottleneck. *Advances in neural information processing systems*, 32, 2019.
- [17] Sham Kakade and John Langford. Approximately optimal approximate reinforcement learning. In *In Proc. 19th International Conference on Machine Learning (ICML)*. Citeseer, 2002.

- [18] Alex Kendall, Jeffrey Hawke, David Janz, Przemyslaw Mazur, Daniele Reda, John-Mark Allen, Vinh-Dieu Lam, Alex Bewley, and Amar Shah. Learning to drive in a day. In *2019 International Conference on Robotics and Automation (ICRA)*, pages 8248–8254. IEEE, 2019.
- [19] Robert Kirk, Amy Zhang, Edward Grefenstette, and Tim Rocktäschel. A survey of generalisation in deep reinforcement learning. *arXiv preprint arXiv:2111.09794*, 2021.
- [20] Aviral Kumar, Xue Bin Peng, and Sergey Levine. Reward-conditioned policies. *arXiv preprint arXiv:1912.13465*, 2019.
- [21] Michael Laskin, Aravind Srinivas, and Pieter Abbeel. Curl: Contrastive unsupervised representations for reinforcement learning. In *International Conference on Machine Learning*, pages 5639–5650. PMLR, 2020.
- [22] Kimin Lee, Kibok Lee, Jinwoo Shin, and Honglak Lee. Network randomization: A simple technique for generalization in deep reinforcement learning. In *International Conference on Learning Representations*, 2019.
- [23] Kimin Lee, Younggyo Seo, Seunghyun Lee, Honglak Lee, and Jinwoo Shin. Context-aware dynamics model for generalization in model-based reinforcement learning. In *International Conference on Machine Learning*, pages 5757–5766. PMLR, 2020.
- [24] Kuang-Huei Lee, Ofir Nachum, Mengjiao Sherry Yang, Lisa Lee, Daniel Freeman, Sergio Guadarrama, Ian Fischer, Winnie Xu, Eric Jang, Henryk Michalewski, et al. Multi-game decision transformers. *Advances in Neural Information Processing Systems*, 35:27921–27936, 2022.
- [25] Vincent Micheli, Eloi Alonso, and François Fleuret. Transformers are sample-efficient world models. In *Deep Reinforcement Learning Workshop NeurIPS 2022*, 2022.
- [26] Volodymyr Mnih, Koray Kavukcuoglu, David Silver, Andrei A. Rusu, Joel Veness, Marc G. Bellemare, Alex Graves, Martin A. Riedmiller, Andreas Fidjeland, Georg Ostrovski, Stig Petersen, Charles Beattie, Amir Sadik, Ioannis Antonoglou, Helen King, Dharshan Kumaran, Daan Wierstra, Shane Legg, and Demis Hassabis. Human-level control through deep reinforcement learning. *Nature*, 518(7540):529–533, 2015.
- [27] Yao Mark Mu, Shoufa Chen, Mingyu Ding, Jianyu Chen, Runjian Chen, and Ping Luo. Ctrl-former: Learning transferable state representation for visual control via transformer. In *International Conference on Machine Learning*, pages 16043–16061. PMLR, 2022.
- [28] Tung D Nguyen, Rui Shu, Tuan Pham, Hung Bui, and Stefano Ermon. Temporal predictive coding for model-based planning in latent space. In *International Conference on Machine Learning*, pages 8130–8139. PMLR, 2021.
- [29] Masashi Okada and Tadahiro Taniguchi. Dreaming: Model-based reinforcement learning by latent imagination without reconstruction. In *2021 IEEE International Conference on Robotics and Automation (ICRA)*, pages 4209–4215. IEEE, 2021.
- [30] Minting Pan, Xiangming Zhu, Yunbo Wang, and Xiaokang Yang. Iso-dream: Isolating non-controllable visual dynamics in world models. In *Advances in Neural Information Processing Systems*, 2022.
- [31] Roberta Raileanu and Rob Fergus. Decoupling value and policy for generalization in reinforcement learning. In *International Conference on Machine Learning*, pages 8787–8798. PMLR, 2021.
- [32] Roberta Raileanu, Maxwell Goldstein, Denis Yarats, Ilya Kostrikov, and Rob Fergus. Automatic data augmentation for generalization in reinforcement learning. *Advances in Neural Information Processing Systems*, 34:5402–5415, 2021.
- [33] Kate Rakelly, Aurick Zhou, Chelsea Finn, Sergey Levine, and Deirdre Quillen. Efficient off-policy meta-reinforcement learning via probabilistic context variables. In *International conference on machine learning*, pages 5331–5340. PMLR, 2019.

- [34] Jan Robine, Marc Höftmann, Tobias Uelwer, and Stefan Harmeling. Transformer-based world models are happy with 100k interactions. *arXiv preprint arXiv:2303.07109*, 2023.
- [35] John Schulman, Philipp Moritz, Sergey Levine, Michael Jordan, and Pieter Abbeel. High-dimensional continuous control using generalized advantage estimation. *arXiv preprint arXiv:1506.02438*, 2015.
- [36] Ramanan Sekar, Oleh Rybkin, Kostas Daniilidis, Pieter Abbeel, Danijar Hafner, and Deepak Pathak. Planning to explore via self-supervised world models. In *International Conference on Machine Learning*, pages 8583–8592. PMLR, 2020.
- [37] Younggyo Seo, Kimin Lee, Stephen L James, and Pieter Abbeel. Reinforcement learning with action-free pre-training from videos. In *International Conference on Machine Learning*, pages 19561–19579. PMLR, 2022.
- [38] David Silver, Aja Huang, Chris J. Maddison, Arthur Guez, Laurent Sifre, George van den Driessche, Julian Schrittwieser, Ioannis Antonoglou, Vedavyas Panneshelvam, Marc Lanctot, Sander Dieleman, Dominik Grewe, John Nham, Nal Kalchbrenner, Ilya Sutskever, Timothy P. Lillicrap, Madeleine Leach, Koray Kavukcuoglu, Thore Graepel, and Demis Hassabis. Mastering the game of go with deep neural networks and tree search. *Nature*, 529(7587):484–489, 2016.
- [39] Shagun Sodhani, Amy Zhang, and Joelle Pineau. Multi-task reinforcement learning with context-based representations. In *International Conference on Machine Learning*, pages 9767–9779. PMLR, 2021.
- [40] Xingyou Song, Yiding Jiang, Stephen Tu, Yilun Du, and Behnam Neyshabur. Observational overfitting in reinforcement learning. In *International Conference on Learning Representations*, 2019.
- [41] Richard S Sutton and Andrew G Barto. *Reinforcement learning: An introduction*. MIT press, 2018.
- [42] Yuval Tassa, Yotam Doron, Alistair Muldal, Tom Erez, Yazhe Li, Diego de Las Casas, David Budden, Abbas Abdolmaleki, Josh Merel, Andrew Lefrancq, et al. Deepmind control suite. *arXiv preprint arXiv:1801.00690*, 2018.
- [43] Emanuel Todorov, Tom Erez, and Yuval Tassa. Mujoco: A physics engine for model-based control. In *2012 IEEE/RSJ international conference on intelligent robots and systems*, pages 5026–5033. IEEE, 2012.
- [44] Laurens Van der Maaten and Geoffrey Hinton. Visualizing data using t-sne. *Journal of machine learning research*, 9(11), 2008.
- [45] Ashish Vaswani, Noam Shazeer, Niki Parmar, Jakob Uszkoreit, Llion Jones, Aidan N Gomez, Łukasz Kaiser, and Illia Polosukhin. Attention is all you need. *Advances in neural information processing systems*, 30, 2017.
- [46] Jane X Wang, Michael King, Nicolas Porcel, Zeb Kurth-Nelson, Tina Zhu, Charlie Deck, Peter Choy, Mary Cassin, Malcolm Reynolds, Francis Song, et al. Alchemy: A benchmark and analysis toolkit for meta-reinforcement learning agents. *arXiv preprint arXiv:2102.02926*, 2021.
- [47] Jane X Wang, Zeb Kurth-Nelson, Dhruva Tirumala, Hubert Soyer, Joel Z Leibo, Remi Munos, Charles Blundell, Dharshan Kumaran, and Matt Botvinick. Learning to reinforcement learn. *arXiv preprint arXiv:1611.05763*, 2016.
- [48] Kaixin Wang, Bingyi Kang, Jie Shao, and Jiashi Feng. Improving generalization in reinforcement learning with mixture regularization. *Advances in Neural Information Processing Systems*, 33:7968–7978, 2020.
- [49] Tongzhou Wang, Simon Du, Antonio Torralba, Phillip Isola, Amy Zhang, and Yuandong Tian. Denoised mdps: Learning world models better than the world itself. In *International Conference on Machine Learning*, pages 22591–22612. PMLR, 2022.

- [50] Yingchen Xu, Jack Parker-Holder, Aldo Pacchiano, Philip J Ball, Oleh Rybkin, Stephen J Roberts, Tim Rocktäschel, and Edward Grefenstette. Learning general world models in a handful of reward-free deployments. *arXiv preprint arXiv:2210.12719*, 2022.
- [51] Ruihan Yang, Huazhe Xu, Yi Wu, and Xiaolong Wang. Multi-task reinforcement learning with soft modularization. *Advances in Neural Information Processing Systems*, 33:4767–4777, 2020.
- [52] Denis Yarats, Amy Zhang, Ilya Kostrikov, Brandon Amos, Joelle Pineau, and Rob Fergus. Improving sample efficiency in model-free reinforcement learning from images. In *Proceedings of the AAAI Conference on Artificial Intelligence*, volume 35, pages 10674–10681, 2021.
- [53] Chengyang Ying, Xinning Zhou, Hang Su, Dong Yan, Ning Chen, and Jun Zhu. Towards safe reinforcement learning via constraining conditional value-at-risk. *arXiv preprint arXiv:2206.04436*, 2022.
- [54] Chiyuan Zhang, Oriol Vinyals, Remi Munos, and Samy Bengio. A study on overfitting in deep reinforcement learning. *arXiv preprint arXiv:1804.06893*, 2018.
- [55] Chenyang Zhao, Olivier Sigaud, Freek Stulp, and Timothy M Hospedales. Investigating generalisation in continuous deep reinforcement learning. *arXiv preprint arXiv:1902.07015*, 2019.

A Pseudo Code of TAD

Algorithm 2 Task Aware Dreamer (TAD)

Require: M training tasks $\{\mathcal{M}_m\}_{m=1}^M$, M replay buffers $\{\mathcal{D}_m\}_{m=1}^M$, N testing tasks $\{\mathcal{M}_{M+n}\}_{n=1}^N$, initialize neural network parameters of world models, the policy, and the critic

- 1: **while** not converge **do**
- 2: //Model Training
- 3: **for** update step = 1, 2, ..., U **do**
- 4: Sample observation-action-reward pairs from each replay buffer $\{(o_t^i, a_t^i, r_t^i)^T\}_{i=1}^T \sim \mathcal{D}_i, i = 1, 2, \dots, M$
- 5: Calculate the deterministic state h and further calculate model states s .
- 6: Update the world models via optimizing Eq. (6).
- 7: Collect imagined trajectories from each s_t via the policy and the world models.
- 8: Use these imagined trajectories to update the policy and the critic.
- 9: **end for**
- 10: //Data Collection
- 11: **for** $m = 1, 2, \dots, M$ **do**
- 12: $o_1 \leftarrow \mathcal{M}_m.reset()$
- 13: **for** sample step = 1, 2, ..., S **do**
- 14: Compute h_t, s_t and sample action a_t via the policy.
- 15: $r_t, o_{t+1} \leftarrow \mathcal{M}_m.step(a_t)$
- 16: **end for**
- 17: Add these data to the replay buffer \mathcal{D}_m .
- 18: **end for**
- 19: **end while**
- 20: //Model Evaluation
- 21: **for** $n = 1, 2, \dots, N$ **do**
- 22: $o_1 \leftarrow \mathcal{M}_{M+n}.reset()$
- 23: **while** the environment not done **do**
- 24: Compute h_t, s_t and sample action a_t via the policy.
- 25: $r_t, o_{t+1} \leftarrow \mathcal{M}_{M+n}.step(a_t)$
- 26: **end while**
- 27: **end for**

B Proof of Theorems

In this section, we will provide detailed proofs of theorems in the paper.

B.1 The Proof of Theorem 1

Proof. We first prove that for $\forall \pi \in \Pi_2$, we have $\mathbb{E}_{\mathcal{M} \sim \mathcal{T}}[J_{\mathcal{M}}(\pi)] = J_{\bar{\mathcal{M}}}(\pi)$.

For any $\mathcal{M} = (\mathcal{S}, \mathcal{A}, \mathcal{P}, \mathcal{R}_{\mathcal{M}}, \gamma) \sim \mathcal{T}$, we can use the policy π to interact with \mathcal{M} and get the trajectory $\tau = (s_0^{\mathcal{M}}, a_0^{\mathcal{M}}, r_1^{\mathcal{M}}, s_1^{\mathcal{M}}, a_1^{\mathcal{M}}, r_2^{\mathcal{M}}, \dots)$. Since the dynamic transition \mathcal{P} is the same for all \mathcal{M} and the policy $\pi \in \Pi_2$ only depends on historical states and actions, we naturally have that the distribution of all states and actions $(s_0^{\mathcal{M}}, a_0^{\mathcal{M}}, s_1^{\mathcal{M}}, a_1^{\mathcal{M}}, \dots)$ are the same for all $\mathcal{M} \sim \mathcal{T}$ as well as $\bar{\mathcal{M}}$. Consequently, we have

$$\begin{aligned}
\mathbb{E}_{\mathcal{M} \sim \mathcal{T}}[J_{\mathcal{M}}(\pi)] &= \mathbb{E}_{\mathcal{M} \sim \mathcal{T}} \mathbb{E}_{\tau \sim \mathcal{P}, \pi}[R_{\mathcal{M}}(\tau)] = \mathbb{E}_{\mathcal{M} \sim \mathcal{T}} \mathbb{E}_{\tau \sim \mathcal{P}, \pi} \left[\sum_{t=0}^{\infty} \gamma^t r_t^{\mathcal{M}} \right] \\
&= \mathbb{E}_{\tau \sim \mathcal{P}, \pi} \left[\sum_{t=0}^{\infty} \gamma^t \mathbb{E}_{\mathcal{M} \sim \mathcal{T}}[r_t^{\mathcal{M}}] \right] = \mathbb{E}_{\tau \sim \mathcal{P}, \pi} \left[\sum_{t=0}^{\infty} \gamma^t \mathbb{E}_{\mathcal{M} \sim \mathcal{T}}[\mathcal{R}_{\mathcal{M}}(s_t^{\mathcal{M}}, a_t^{\mathcal{M}})] \right] \quad (7) \\
&= \mathbb{E}_{\tau \sim \mathcal{P}, \pi} \left[\sum_{t=0}^{\infty} \gamma^t [\bar{\mathcal{R}}(s_t^{\mathcal{M}}, a_t^{\mathcal{M}})] \right] = \mathbb{E}_{\tau \sim \mathcal{P}, \pi}[R_{\bar{\mathcal{M}}}(\tau)] = J_{\bar{\mathcal{M}}}(\pi).
\end{aligned}$$

It is well known that the optimal policy in single MDP is memory-less, i.e., $\max_{\pi \in \Pi_2} J_{\mathcal{M}}(\pi) = \max_{\pi \in \Pi_1} J_{\mathcal{M}}(\pi)$. Consequently, we have

$$\begin{aligned}
J_{\mathcal{T}}^2 &= \max_{\pi \in \Pi_2} \mathbb{E}_{\mathcal{M} \sim \mathcal{T}} [J_{\mathcal{M}}(\pi)] = \max_{\pi \in \Pi_2} J_{\mathcal{M}}(\pi) \\
&= \max_{\pi \in \Pi_1} J_{\mathcal{M}}(\pi) = \max_{\pi \in \Pi_1} \mathbb{E}_{\mathcal{M} \sim \mathcal{T}} [J_{\mathcal{M}}(\pi)] = J_{\mathcal{T}}^1 \\
&\leq \mathbb{E}_{\mathcal{M} \sim \mathcal{T}} \left[\max_{\pi \in \Pi_1} J_{\mathcal{M}}(\pi) \right] = J_{\mathcal{T}}^*.
\end{aligned} \tag{8}$$

Thus we have proven this result. \square

B.2 The Proof of Theorem 2

Proof. Our proof follows some previous work [17, 53]. First, we consider the bellman equation of value function of $\pi, \pi_{\mathcal{M}}^* \in \Pi_1$ in \mathcal{M} as

$$\begin{aligned}
V_{\mathcal{M}, \pi}(s) &= \sum_a \pi(a|s) \left[\mathcal{R}(s, a) + \gamma \sum_{s'} \mathcal{P}(s'|s, a) V_{\mathcal{M}, \pi}(s') \right], \\
V_{\mathcal{M}, \pi_{\mathcal{M}}^*}(s) &= \sum_a \pi_{\mathcal{M}}^*(a|s) \left[\mathcal{R}(s, a) + \gamma \sum_{s'} \mathcal{P}(s'|s, a) V_{\mathcal{M}, \pi_{\mathcal{M}}^*}(s') \right].
\end{aligned}$$

Defining $\Delta V(s) \triangleq V_{\mathcal{M}, \pi}(s) - V_{\mathcal{M}, \pi_{\mathcal{M}}^*}(s)$ as the difference of these two value functions, we can further deduce that

$$\begin{aligned}
\Delta V(s) &= V_{\mathcal{M}, \pi}(s) - V_{\mathcal{M}, \pi_{\mathcal{M}}^*}(s) \\
&= \gamma \sum_a \Delta \pi(a|s) \sum_{s'} \mathcal{P}(s'|s, a) V_{\mathcal{M}, \pi_{\mathcal{M}}^*}(s') + \gamma \sum_a \pi(a|s) \sum_{s'} \mathcal{P}(s'|s, a) \Delta V(s') \\
&\quad + \sum_a \Delta \pi(a|s) \mathcal{R}(s, a) \\
&= \sum_a \Delta \pi(a|s) Q_{\mathcal{M}, \pi_{\mathcal{M}}^*}(s, a) + \gamma \sum_a \pi(a|s) \sum_{s'} \mathcal{P}(s'|s, a) \Delta V(s'),
\end{aligned} \tag{9}$$

here $\Delta \pi(a|s) = \pi(a|s) - \pi_{\mathcal{M}}^*(a|s)$. Since Eq. (9) holds for any s , thus we calculate its expectation for $s \sim d_{\mathcal{M}}^{\pi}$:

$$\begin{aligned}
&\sum_s d_{\mathcal{M}}^{\pi}(s) \Delta V(s) \\
&= \sum_s d_{\mathcal{M}}^{\pi}(s) [V_{\mathcal{M}, \pi}(s) - V_{\mathcal{M}, \pi_{\mathcal{M}}^*}(s)] \\
&= \sum_s d_{\mathcal{M}}^{\pi}(s) \sum_a \Delta \pi(a|s) Q_{\mathcal{M}, \pi_{\mathcal{M}}^*}(s, a) + \gamma \sum_s d_{\mathcal{M}}^{\pi}(s) \sum_a \pi(a|s) \sum_{s'} \mathcal{P}(s'|s, a) \Delta V(s') \\
&= \sum_s d_{\mathcal{M}}^{\pi}(s) \sum_a \Delta \pi(a|s) Q_{\mathcal{M}, \pi_{\mathcal{M}}^*}(s, a) + \sum_{s'} \Delta V(s') \left[\gamma \sum_s d_{\mathcal{M}}^{\pi}(s) \sum_a \pi(a|s) \mathcal{P}(s'|s, a) \right].
\end{aligned} \tag{10}$$

Since $d_{\mathcal{M}}^{\pi}(s) - (1 - \gamma) \mathcal{P}(s_0 = s) = \gamma \sum_{s'} d_{\mathcal{M}}^{\pi}(s') \sum_a \pi(a|s') \mathcal{P}(s|s', a)$, we can further prove that

$$\begin{aligned}
\sum_s d_{\mathcal{M}}^{\pi}(s) \Delta V(s) &= \sum_s d_{\mathcal{M}}^{\pi}(s) \sum_a \Delta \pi(a|s) Q_{\mathcal{M}, \pi_{\mathcal{M}}^*}(s, a) \\
&\quad + \sum_{s'} \Delta V(s') [d_{\mathcal{M}}^{\pi}(s') - (1 - \gamma) \mathcal{P}(s_0 = s')].
\end{aligned} \tag{11}$$

By moving the second term of the right part in Eq. (11) to the left part, we can deduce that

$$(1 - \gamma) \sum_{s'} \Delta V(s') \mathcal{P}(s_0 = s') = \sum_s d_{\mathcal{M}}^{\pi}(s) \sum_a \Delta \pi(a|s) Q_{\mathcal{M}, \pi_{\mathcal{M}}^*}(s, a), \tag{12}$$

thus we can calculate that

$$\begin{aligned}
J_{\mathcal{M}}(\pi) - J_{\mathcal{M}}(\pi_{\mathcal{M}}^*) &= \sum_{s'} \Delta V(s') \mathcal{P}(s_0 = s') = \frac{1}{1-\gamma} \sum_s d_{\mathcal{M}}^{\pi}(s) \sum_a \Delta \pi(a|s) Q_{\mathcal{M}, \pi_{\mathcal{M}}^*}(s, a) \\
&= \frac{1}{1-\gamma} \sum_s d_{\mathcal{M}}^{\pi}(s) \sum_a [\pi(a|s) - \pi_{\mathcal{M}}^*(a|s)] Q_{\mathcal{M}, \pi_{\mathcal{M}}^*}(s, a) \\
&= \frac{1}{1-\gamma} \mathbb{E}_{s \sim d_{\mathcal{M}}^{\pi}} \mathbb{E}_{a \sim \pi(\cdot|s)} \left(1 - \frac{\pi_{\mathcal{M}}^*(a|s)}{\pi(a|s)} \right) Q_{\mathcal{M}, \pi_{\mathcal{M}}^*}(s, a) \\
&= \frac{1}{1-\gamma} \mathbb{E}_{s \sim d_{\mathcal{M}}^{\pi}} \int_{\mathcal{A}} \pi(a|s) \left(1 - \frac{\pi_{\mathcal{M}}^*(a|s)}{\pi(a|s)} \right) Q_{\mathcal{M}}^*(s, a) da \\
&= \frac{1}{1-\gamma} \mathbb{E}_{s \sim d_{\mathcal{M}}^{\pi}} \left[\int_a \pi(a|s) Q_{\mathcal{M}}^*(s, a) da - \max_a Q_{\mathcal{M}}^*(s, a) \right].
\end{aligned} \tag{13}$$

Consequently, we have

$$\begin{aligned}
\mathbb{E}_{\mathcal{M} \sim \mathcal{T}} [J_{\mathcal{M}}(\pi_{\mathcal{M}}^*) - J_{\mathcal{M}}(\pi)] &= \frac{1}{1-\gamma} \mathbb{E}_{\mathcal{M} \sim \mathcal{T}} \mathbb{E}_{s \sim d_{\mathcal{M}, \pi(\cdot)}} \left[\max_a Q_{\mathcal{M}}^*(s, a) - \int_a \pi(a|s) Q_{\mathcal{M}}^*(s, a) da \right] \\
&\geq \frac{1}{1-\gamma} \mathbb{E}_{s \sim d_{\mathcal{M}, \pi(\cdot)}} \left[\mathbb{E}_{\mathcal{M} \sim \mathcal{T}} \max_a Q_{\mathcal{M}}^*(s, a) - \max_a \mathbb{E}_{\mathcal{M} \sim \mathcal{T}} Q_{\mathcal{M}}^*(s, a) \right] \\
&= \frac{1}{1-\gamma} \mathbb{E}_{s \sim d_{\mathcal{M}, \pi}} [D_{\text{TDR}}(\mathcal{T}, s)].
\end{aligned} \tag{14}$$

Since $J_{\mathcal{M}}(\pi_{\mathcal{M}}^*) = \max_{\pi \in \Pi_1} J_{\mathcal{M}}(\pi)$, we have

$$\mathbb{E}_{\mathcal{M} \sim \mathcal{T}} \max_{\pi \in \Pi_1} J_{\mathcal{M}}(\pi) - \max_{\pi \in \Pi_1} \mathbb{E}_{\mathcal{M} \sim \mathcal{T}} J_{\mathcal{M}}(\pi) \geq \frac{1}{1-\gamma} \mathbb{E}_{s \sim d_{\mathcal{M}, \pi^*}} [D_{\text{TDR}}(\mathcal{T}, s)], \tag{15}$$

Thus we have proven this result. \square

B.3 Expressive Ability of Π_3

Proposition 1. For $\forall \epsilon_1, \epsilon_2$ satisfying $0 < \epsilon_1 \leq 1, 0 < \epsilon_2 \leq 1$, there exists a task distribution \mathcal{T} satisfying that

$$J_{\mathcal{T}}^1 = J_{\mathcal{T}}^2 \leq \epsilon_1, \quad J_{\mathcal{T}}^3 \geq 1 - \epsilon_2, \quad J_{\mathcal{T}}^* = 1. \tag{16}$$

Proof. Given fixed discount factor $\gamma \in (0, 1)$, we first take $n \in \mathbb{N}$ satisfying $n \geq \frac{1}{\epsilon_1}$, $A = \epsilon_2 \frac{n}{n-1} \frac{1-\gamma}{1-\gamma^n}$, and $B = \frac{1-\gamma}{\gamma^{n+1}} \left(1 - \epsilon_2 \frac{n}{n-1} \right)$. We construct state sets $\mathcal{S} = \{s_t^l\} (t = 0, 1, \dots, \infty, l = 1, \dots, n)$ and action sets $\mathcal{A} = \{a_j\}_{j=1}^n$. Then we construct n tasks $\mathcal{M}_i = (\mathcal{S}, \mathcal{A}, \mathcal{P}, \mathcal{R}_i, \gamma), i = 1, \dots, n$, which share the same dynamic \mathcal{P} and different reward functions \mathcal{R}_i . The initial state of each task is s_0^1 , and the dynamic as well as reward functions are as below

$$\begin{aligned}
\mathcal{P}(s_t^l, a_j) &= \mathbb{I}(s = s_{t+1}^j), \quad j = 1, \dots, n; \quad l = 1, \dots, n; \quad t = 0, 1, \dots, \infty \\
\mathcal{R}_i(s_t^l, a_j) &= f(t) \mathbb{I}(i = j), \quad i, j = 1, \dots, n; \quad l = 1, \dots, n; \quad t = 0, 1, \dots, \infty \\
f(t) &= \begin{cases} A, & t \leq n-1 \\ B, & t \geq n \end{cases}
\end{aligned} \tag{17}$$

Take \mathcal{T} as the uniform distribution over $\mathcal{M}_1, \dots, \mathcal{M}_n$, thus we have

$$\begin{aligned}
J_{\mathcal{M}_i}^* &= A + A\gamma + \dots + A\gamma^{n-1} + B\gamma^n + B\gamma^{n+1} + \dots \\
&= A \frac{1-\gamma^n}{1-\gamma} + B \frac{\gamma^{n+1}}{1-\gamma} = 1 \\
J_{\mathcal{T}}^* &= \frac{1}{n} \sum_{i=1}^n J_{\mathcal{M}_i}^* = 1.
\end{aligned} \tag{18}$$

Since our construction satisfies $\mathbb{E}_{\mathcal{T}}[\mathcal{R}_i(s_k^l, a_j)] = \frac{f(k)}{n}$, for $\forall \pi \in \Pi_2$, we have

$$\begin{aligned} J_{\mathcal{T}}(\pi) &= \frac{1}{n}(A + A\gamma + \dots + A\gamma^{n-1} + B\gamma^n + B\gamma^{n+1} + \dots) = \frac{1}{n}, \\ J_{\mathcal{T}}^1 &= J_{\mathcal{T}}^2 = \max_{\pi \in \Pi_2} J_{\mathcal{T}}(\pi) = \frac{1}{n} \leq \epsilon_1. \end{aligned} \quad (19)$$

Moreover, we can construction an agent $\hat{\pi} \in \Pi_3$ that takes action via the historical trajectory $\hat{r}_t = (\hat{s}_0, \hat{a}_0, \hat{r}_0, \dots, \hat{s}_t)$:

$$\begin{aligned} \hat{\pi}(a_j | \hat{r}_t) &= \mathbb{I}(j = t + 1), \quad t = 0, 1, \dots, n - 1 \\ \hat{\pi}(a_j | \hat{r}_t) &= \mathbb{I}(j = i), \quad t = n, \dots, \infty \end{aligned} \quad (20)$$

here $i = \arg \max\{\hat{r}_0, \hat{r}_1, \dots, \hat{r}_{n-1}\} + 1$, thus we have

$$\begin{aligned} J_{\mathcal{T}}^3 &\geq J_{\mathcal{T}}(\hat{\pi}) = \frac{1}{n}(A + A\gamma + \dots + A\gamma^{n-1}) + B\gamma^n + B\gamma^{n+1} + \dots \\ &= \frac{A}{n} \frac{1 - \gamma^n}{1 - \gamma} + B \frac{\gamma^{n+1}}{1 - \gamma} = 1 - \frac{(n-1)A}{n} \frac{1 - \gamma^n}{1 - \gamma} \\ &\geq 1 - \epsilon_2. \end{aligned} \quad (21)$$

Thus we have proven this result. \square

B.4 The Derivation of the Inequality (5)

We have

$$\begin{aligned} &\ln p(o_{1:T}, r_{1:T}, \mathcal{M} | a_{1:T}) \\ &= \ln \mathbb{E}_{p(s_{1:T} | a_{1:T})} [p(o_{1:T}, r_{1:T}, \mathcal{M} | s_{1:T})] \\ &= \ln \mathbb{E}_{p(s_{1:T} | a_{1:T})} [p(o_{1:T}, r_{1:T} | \mathcal{M}, s_{1:T}) p(\mathcal{M} | s_{1:T})] \\ &= \ln \mathbb{E}_{p(s_{1:T} | a_{1:T})} \left[p(\mathcal{M} | s_{1:T}) \prod_{t=1}^T p(o_t, r_t | \mathcal{M}, s_t) \right] \\ &= \ln \mathbb{E}_{q(s_{1:T} | o_{1:T}, a_{1:T}, r_{1:T})} \left[p(\mathcal{M} | s_{1:T}) \prod_{t=1}^T p(o_t, r_t | \mathcal{M}, s_t) \frac{p(s_t | s_{t-1}, a_{t-1})}{q(s_t | o_{\leq t}, r_{< t}, a_{< t})} \right] \\ &\geq \mathbb{E}_{q(s_{1:T} | o_{1:T}, a_{1:T}, r_{1:T})} [\ln p(\mathcal{M} | s_{1:T})] \\ &\quad + \mathbb{E}_{q(s_{1:T} | o_{1:T}, a_{1:T}, r_{1:T})} \sum_{t=1}^T [\ln p(o_t, r_t | \mathcal{M}, s_t) + \ln p(s_t | s_{t-1}, a_{t-1}) - \ln q(s_t | o_{\leq t}, r_{< t}, a_{< t})] \\ &= \mathbb{E}_{q(s_{1:T} | o_{1:T}, a_{1:T}, r_{1:T})} [\ln p(\mathcal{M} | s_{1:T})] \\ &\quad + \sum_{t=1}^T \left[\mathbb{E}_{q(s_{1:T} | o_{1:T}, a_{1:T}, r_{1:T})} \ln p(o_t, r_t | \mathcal{M}, s_t) - \mathbb{E}_{q(s_{1:T} | o_{1:T}, a_{1:T}, r_{1:T})} \ln \frac{q(s_t | o_{\leq t}, r_{< t}, a_{< t})}{p(s_t | s_{t-1}, a_{t-1})} \right] \\ &= \mathbb{E}_{q(s_{1:T} | o_{1:T}, a_{1:T}, r_{1:T})} [\ln p(\mathcal{M} | s_{1:T})] + \sum_{t=1}^T \mathbb{E}_{q(s_t | o_{\leq t}, a_{< t}, r_{< t})} [\ln p(o_t, r_t | \mathcal{M}, s_t)] \\ &\quad - \sum_{t=1}^T \mathbb{E}_{q(s_t | o_{\leq t}, r_{< t}, a_{< t})} \mathbb{E}_{q(s_{t-1} | o_{\leq (t-1)}, r_{< (t-1)}, a_{< (t-1)})} \left[\ln \frac{q(s_t | o_{\leq t}, r_{< t}, a_{< t})}{p(s_t | s_{t-1}, a_{t-1})} \right] \\ &= \mathbb{E}_{q(s_{1:T} | o_{1:T}, a_{1:T}, r_{1:T})} [\ln p(\mathcal{M} | s_{1:T})] + \sum_{t=1}^T \mathbb{E}_{q(s_t | o_{\leq t}, a_{< t}, r_{< t})} [\ln p(o_t, r_t | \mathcal{M}, s_t)] \\ &\quad - \sum_{t=1}^T \mathbb{E}_{q(s_{t-1} | o_{\leq (t-1)}, r_{< (t-1)}, a_{< (t-1)})} [\text{KL}(q(s_t | o_{\leq t}, r_{< t}, a_{< t}) || p(s_t | s_{t-1}, a_{t-1}))]. \end{aligned} \quad (22)$$

Thus we have proven the inequality (5).

B.5 Sparse Reward Task

In this part, we show that generalizing to tasks with the same dynamics and sparse rewards without extra knowledge (like context) is extremely difficult and sometimes impossible. It is because we cannot distinguish them via historical information. Here we construct an example.

Assume there are n MDPs, $\mathcal{M}_i (i = 1, \dots, n)$, each MDP share the same state set $\mathcal{S} = \{s_1, \dots, s_T\}$ and action set $\mathcal{A} = \{a_1, \dots, a_n\}$. The initial state is s_1 and the dynamic is that $\mathcal{P}(s_{t+1}|s_t, a_i) = 1 (t = 1, \dots, T - 1, i = 1, \dots, n)$, $\mathcal{P}(s_T|s_T, a_i) = 1 (i = 1, \dots, n)$. As for the reward function, we define that

$$\mathcal{R}_{\mathcal{M}_i}(s_{T-1}, a_i) = 1, i = 1, \dots, n. \quad (23)$$

and the reward function is 0 otherwise. In this case, any policies (including markovian, state-action memorized, and state-action-reward memorized) in this task distribution can only handle one task since they can not distinguish them.

C Experimental Details for DMControl

In this part, we first *roughly* discuss the reward function of tasks in our experiments to better understand their TDR. These reward functions always defined by tolerance function in DeepMind control suite [42], which is a smooth function with parameters $\text{tolerance}(x, \text{bounds} = (\text{lower}, \text{upper}))$ and hope the value of x is within (lower, upper). More details about tolerance function can be found in [42].

- **Walker-stand&walk.** This task combination includes two tasks: Walker-stand and Walker-walk, which both require a two-leg robot to maintain its height above a certain threshold, and Walker-walk also hopes it to move faster than a certain speed, i.e., their reward functions can be roughly described as

$$\begin{aligned} \mathcal{R}_{\text{stand}} &= \text{tolerance}(\text{height}, (1.2, \infty)), \\ \mathcal{R}_{\text{walk}} &= \text{tolerance}(\text{height}, (1.2, \infty)) * \text{tolerance}(\text{speed}, (1, \infty)). \end{aligned} \quad (24)$$

Therefore, for all states, the optimal action of Walker-walk is also optimal in Walker-stand and TDR here is 0.

- **Cartpole-balance&sparse.** This task combination includes two tasks: Cartpole-balance and Cartpole-balance_sparse, which both hope to balance an unactuated pole with dense and sparse rewards respectively. The optimal actions of these tasks are both hope to balance the agent and thus TDR here is 0.
- **Acrobot-swingup&sparse.** This task combination includes two tasks: Acrobot-swingup and Acrobot-swingup_sparse, which both hope to swing up a double pendulum with dense and sparse rewards respectively. Also, the optimal actions of these tasks are both hoped to swingup the agent and thus TDR here is 0.
- **Quadruped-walk&run.** This task combination includes two tasks: Quadruped-walk and Quadruped-run, which both require a quadruped agent to move faster than a target speed. The target speed of the running task is larger than the walking task, i.e., their reward functions can be roughly described as

$$\begin{aligned} \mathcal{R}_{\text{walk}} &= \text{tolerance}(\text{speed}, (0.5, \infty)), \\ \mathcal{R}_{\text{run}} &= \text{tolerance}(\text{speed}, (5.0, \infty)). \end{aligned} \quad (25)$$

Therefore, TDR here is still 0 since optimal actions of Quadruped-run are also optimal in Quadruped-walk.

- **Reacher-easy&hard.** This task combination includes two tasks: Reacher-easy and Reacher-hard, which both hope to control a two-link planar reacher to prostrate the target sphere. The sizes of target spheres in these two tasks are different, i.e., their reward functions can be roughly described as

$$\begin{aligned} \mathcal{R}_{\text{easy}} &= \text{tolerance}(\text{distance}, (0.0, 0.05)), \\ \mathcal{R}_{\text{hard}} &= \text{tolerance}(\text{distance}, (0.0, 0.015)). \end{aligned} \quad (26)$$

Thus TDR here is not 0 but still small.

- **Hopper-stand&hop.** This task combination includes two tasks: Hopper-stand and Hopper-hop, which both hope the height of a one-legged hopper is larger than the target height. While Hopper-stand hopes the control force is 0, Hopper-hop hopes to control the robot to hop forward and its speed is larger than the target speed. Their reward functions can be roughly described as

$$\begin{aligned}\mathcal{R}_{\text{stand}} &= \text{tolerance}(\text{height}, (0.6, 2)) * \text{tolerance}(\text{speed}, (2.0, \infty)), \\ \mathcal{R}_{\text{hop}} &= \text{tolerance}(\text{height}, (0.6, 2)) * \text{tolerance}(\text{control}, (0.0, 0.0)).\end{aligned}\quad (27)$$

Since one agent can not hop when controlling the force as 0, TDR here is not 0 but not huge.

- **Walker-stand&prostrate.** This task combination includes two tasks: Walker-stand and Walker-prostrate. Walker-stand hopes the height of a two-leg robot to be larger than the target height. And we design the task Walker-prostrate, which hopes its height to be lower than another target height. Their reward functions can be roughly described as

$$\begin{aligned}\mathcal{R}_{\text{stand}} &= \text{tolerance}(\text{height}, (1.2, \infty)), \\ \mathcal{R}_{\text{prostrate}} &= \text{tolerance}(\text{height}, (0.0, 0.2)).\end{aligned}\quad (28)$$

Thus TDR here is huge since the optimal Q functions of these two tasks are almost the opposite.

- **Walker-walk&prostrate.** This task combination includes two tasks: Walker-walk and Walker-prostrate. Walker-walk hopes the height of the improved planar walker to be larger than a target height, while Walker-prostrate hopes it to be lower than a target height. Moreover, Walker-walk hopes the speed of the robot is larger than another target speed, i.e., their reward functions can be roughly described as

$$\begin{aligned}\mathcal{R}_{\text{walk}} &= \text{tolerance}(\text{height}, (1.2, \infty)) * \text{tolerance}(\text{speed}, (1.0, \infty)), \\ \mathcal{R}_{\text{prostrate}} &= \text{tolerance}(\text{height}, (0.0, 0.2)).\end{aligned}\quad (29)$$

Thus TDR here is also huge since the optimal Q functions of these two tasks are almost the opposite.

Now we introduce the three task distributions in our experiments, which are designed based on existing tasks in DeepMind control suite for testing the generalization of trained agents.

- **Cheetah_speed(α, β).** This task distribution is designed in this paper with parameter $0 \leq \beta \leq \alpha$, based on the task Cheetah_run in DeepMind control suite, and hopes the Cheetah robot can run with the target speed interval $(\alpha - \beta, \alpha + \beta)$.

$$\mathcal{R}_{\text{Cheetah_speed}}(\alpha, \beta) = \text{tolerance}(\text{speed}, (\alpha - \beta, \alpha + \beta)).\quad (30)$$

We train the agents in tasks with parameters (0.5, 0.2), (1.5, 0.2), (2.0, 0.2), (3.0, 0.2) and test them in tasks with parameters (1.0, 0.2), (2, 5, 0.2).

- **Pendulum_angle(α, β).** This task distribution is designed in this paper with parameter $-1 \leq \alpha \leq \beta \leq 1$, based on the task Pendulumh_swingup in DeepMind control suite, and hopes the Pendulum robot can swing up within the target angle interval $(\arccos \alpha, \arccos \beta)$.

$$\mathcal{R}_{\text{Pendulum_angle}}(\alpha, \beta) = \text{tolerance}(\text{angle}, (\arccos \alpha, \arccos \beta)).\quad (31)$$

Training tasks are with parameters $(-0.95, -0.9)$, $(-0.85, -0.8)$, $(-0.8, -0.75)$, $(-0.7, -0.65)$ and testing tasks are with parameters $(-0.9, -0.85)$, $(-0, 75, -0.7)$.

- **Quadruped_speed(α, β).** This task distribution is designed in this paper with parameter $0 \leq \beta \leq \alpha$, based on the task Quadruped_run in DeepMind control suite, and hopes the Quadruped robot can run within the target speed interval $(\alpha - \beta, \alpha + \beta)$.

$$\mathcal{R}_{\text{Quadruped_speed}}(\alpha, \beta) = \text{tolerance}(\text{speed}, (\alpha - \beta, \alpha + \beta)).\quad (32)$$

We train the agents in tasks with parameters (0.5, 0.2), (1.5, 0.2), (2.0, 0.2), (3.0, 0.2) and test in tasks with parameters (1.0, 0.2), (2, 5, 0.2).

Moreover, we introduce some details about our experiments. Our codes are based on Python and the deep learning library PyTorch. All algorithms are trained on one NVIDIA GeForce RTX 2080 Ti. As for the hyper-parameters, we follow previous works [10, 12, 11] and select 2 as the action repeat for all experiments following [11].

β	0.2		0.15		0.1	
	Train	Test	Train	Test	Train	Test
Dreamer	250.2 \pm 9.6	3.0 \pm 2.2	247.5 \pm 1.0	0.0 \pm 0.0	175.8 \pm 55.8	13.5 \pm 13.5
TAD	956.8 \pm 6.0	787.4 \pm 163.6	927.6 \pm 2.6	800.1 \pm 121.4	608.5 \pm 321.4	491.6 \pm 389.4

Table 4: Average cumulative reward (mean \pm one std) over different target region (smaller β represents smaller target region and more sparse return) of the best policy trained by Dreamer and TAD in Cheetah_Speed. For each β , we train agents in the train tasks and evaluate them in both train and test environments. Numbers greater than 95 percent of the best performance for each environment are **bold**.

SR	0.0		0.8		0.9	
	Train	Test	Train	Test	Train	Test
Dreamer	250.2 \pm 9.6	3.0 \pm 2.2	237.4 \pm 14.9	28.9 \pm 14.6	168.7 \pm 96.2	157.2 \pm 188.4
TAD	956.8 \pm 6.0	787.4 \pm 163.6	841.9 \pm 154.9	546.1 \pm 291.6	777.7 \pm 170.1	716.8 \pm 136.5

Table 5: Average cumulative reward (mean \pm one std) over different sparse rates of the best policy trained by Dreamer and TAD in Cheetah_Speed. For each sparse rate, we train agents in the train tasks and evaluate them in both train and test environments. Numbers greater than 95 percent of the best performance for each environment are **bold**.

D Experimental Details for MuJoCo

We here introduce state-based control tasks (Half-CheetahFwd-Back, Half-Cheetah-Vel, and Humanoid-Direc-2D) in detail, following the setting of [7, 33].

- **Half-Cheetah-Fwd-Back.** This task distribution includes two tasks: moving forward and moving backward.
- **Half-Cheetah-Vel.** This task distribution hopes the agent to move forward and achieve the target velocity. There are 100 training tasks and 30 testing tasks for experiments.
- **Humanoid-Direc-2D.** This task distribution hopes the agent to move in the target direction. There are 100 training tasks and 30 testing tasks for experiments.

Moreover, we introduce some details about our experiments. Our codes are based on Python and the deep learning library PyTorch. All algorithms are trained on one NVIDIA GeForce RTX 2080 Ti. We select 1 as the action repeat for all experiments following.

E Ablation Study

In this part, we will evaluate TAD in more challenging settings with sparse rewards. First, we evaluate Dreamer and TAD in Cheetah_speed with different β , which identifies the region of target speeds. With smaller β , the reward signals are more sparse since the target intervals are smaller. In the main experiment, we take $\beta = 0.2$, and here we evaluate in $\beta = 0.2, 0.15, 0.1$, of which the result is reported in Table 4. For each β , we take the training parameters $(0.5, \beta)$, $(1.5, \beta)$, $(2.0, \beta)$, $(3.0, \beta)$ and test them in tasks with parameters $(1.0, \beta)$, $(2.5, \beta)$. As shown in Table 4, with the decreasing of β , the performance of Dreamer and TAD decreases since reward signals are sparse so exploration here is much more difficult. However, our TAD still significantly outperforms Dreamer and shows strong generalization abilities, which shows that TAD can effectively utilize historical information, even sparse rewards.

Moreover, we design Cheetah_speed_sparse based on Cheetah_speed. In Cheetah_speed_sparse(n), we make the reward function sparse, i.e., the output reward is the same as Cheetah_speed every n timesteps (in step $n - 1, 2n - 1, \dots$) and 0 otherwise, of which the sparse rate (SR) is $(n - 1)/n$. We supplement experiments to evaluate the performance of Dreamer and TAD with $n = 5$ (SR=0.8) and $n = 10$ (SR=0.9). As shown in Table 5, with the increasing of SR, although the performance of TAD decrease since inferring task context from sparse reward is extremely difficult, TAD still shows strong performance in train tasks and generalizes well to unseen test tasks.

F Ethics Issues and Border Impact

Designing agents which can generalize to unseen tasks is a major concern in reinforcement learning. This work focuses on task generalization in reinforcement learning and proposes a novel algorithm Reward Informed Dreamer. One of the potential negative impacts is that algorithms using deep neural networks, which lack interoperability and theoretical guarantee. If we hope to apply them in real-world applications, they may face security and robustness issues, and a possible way is to develop more explainable methods. There are no serious ethical issues as this is basic research. We hope our work can inspire more research on designing agents with stronger generalization abilities.